RESEARCH ARTICLE SUMMARY

TOPOLOGICAL MATTER

Catalog of topological phonon materials

Yuanfeng Xu*, M. G. Vergniory, Da-Shuai Ma, Juan L. Mañes, Zhi-Da Song, B. Andrei Bernevig*, Nicolas Regnault*, Luis Elcoro*

INTRODUCTION: A crystalline electronic material is topologically nontrivial if its reciprocal-space Bloch states cannot be expressed in terms of localized Wannier functions in real space during an adiabatic process that preserves the crystalline symmetries. In the presence of crystalline or time-reversal symmetries, most of the band topologies can be diagnosed by the Fu-Kane–like topological invariants in terms of the band representations at the high-symmetry momenta. Recently, symmetry-protected topological phases in both the 230 paramagnetic and the 1421 magnetic space groups were exhaustively identified by topological quantum chemistry (TQC) and symmetry-based indicators, which facilitated the construction of catalogs of topological bands in both paramagnetic and magnetic electronic materials. High-throughput calculations classified >50% of the stoichiometric materials in the Inorganic Crystal Structure Database as topological insulators or semimetals at the Fermi level; about 88% had at least one topological band set somewhere in the energy spectrum.

RATIONALE: Phonon structure is another platform for the realization of nontrivial band topologies in solid-state materials. The robustness of the topological surface phonon states can be used for frequency filtering or mechanical energy attenuation under imperfect conditions, for heat transfer, and for infrared photoelectronics. Topological phonons are also promising for the construction of phonon diodes or acoustic waveguides. When time-reversal symmetry is broken, several topological effects, such as quantum anomalous Hall-like or quantum valley Hall-like effects, can be realized in topological phononic materials.

In this work, we fully extended the application of TQC to phonon systems in all the space groups and systematically completed a catalog of topological phonon bands. On the basis of the dynamical matrices of >10,000 materials that were obtained from ab initio calculations and stored in the databases PhononDB@kyoto-u and Materials Project, we performed a comprehensive topological classification for >10,000 phonon band structures with a high-throughput method. For each phonon band structure, we identified the irreducible representations, compatibility relations, topological indices, and real-space invariants. Then, every isolated set of fully connected bands along all the high-symmetry lines and planes in momentum space was diagnosed as topologically nontrivial, as obstructed atomic band representation (OABR), as orbital-selected OABR, or as an atomic set of bands. In addition, we also developed a high-throughput algorithm for the computation of phonon surface states. For each phonon material, we selected three nonequivalent cleavage planes and calculated their surface states with a finite-size slab structure.

RESULTS: Our results show that about half of the materials host at least one nonatomic phonon band set. The percentage of materials hosting nonatomic phonon band sets is not as high as the percentage of materials hosting topological electronic bands with spin-orbit coupling but is higher than the percentage of materials hosting topological electronic bands without spin-orbit coupling. For each isolated phonon band set, although the band structures along all the high-symmetry paths satisfy all the compatibility relations, the nonzero topological indices defined in spinless space groups are necessarily indicating gapless band nodes. Once the Materials Project identification number (MPID) entries tagged as having imaginary phonon frequencies have been removed from the final list, we find 1780 entries in PhononDB@kyoto-u and 151 entries in Materials Project that have all kinds of symmetry-indicated spinless topologies, including Weyl nodes, and nodal lines with and without Z_2-monopole charge. As a side note, we observe a near absence of fragile cumulative topology for phonons. Combined with a numerical analysis of the phonon band structure, we have identified >1000 materials as promising for future experimental analysis. To stimulate the relevant experimental investigation, we also highlight six representative phonon materials with symmetry-indicated topological bands, OABR bands, or symmetry-enforced band nodes.

CONCLUSION: We have performed a comprehensive topological classification for >10,000 phonon materials in a high-throughput search and have made the results available at our public website, the Topological Phonon Database. The database allows the search for the most promising candidates exhibiting nonatomic properties and additional criteria, such as point group or space group symmetry, chemical elements, etc. As phonons are bosonic excitations, topological bandgaps (or band nodes) are not limited to a specific energy level, and the nontrivial topology at any frequency level could be of interest and detectable in experiments. On the basis of the formalism and results of this work, future extension of the catalog of topological phonons may encompass all the solid-state materials contained in the Inorganic Crystal Structure Database. The results of the present work, together with the previous complete analysis of the band topology of the electronic states, will be useful in the analysis of the consequences of electron-phonon coupling on the physical properties of the materials when the topology of both subsystems comes into play. ■

The list of author affiliations is available in the full article online.
*Corresponding author. Email: y.xu@zju.edu.cn (Y.X.); bernevig@princeton.edu (B.A.B.); regnault@princeton.edu (N.R.); luis.elcoro@ehu.eus (L.E.)
Cite this article as Y. Xu *et al.*, *Science* **384**, eadf8458 (2024). DOI: 10.1126/science.adf8458

READ THE FULL ARTICLE AT
https://doi.org/10.1126/science.adf8458

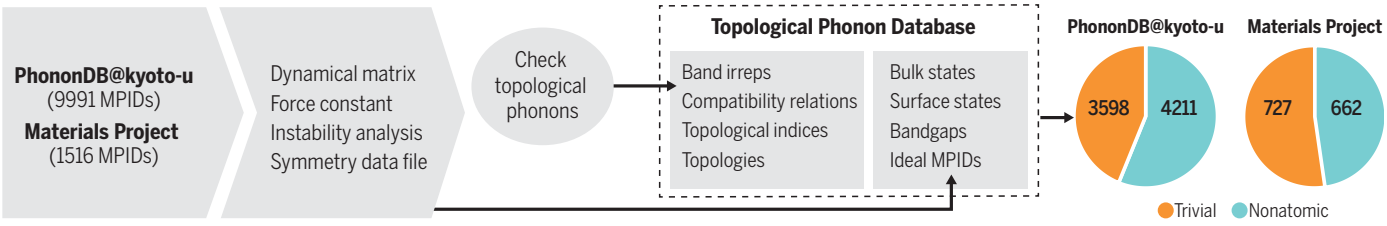

Workflow of the high-throughput calculations. The calculations were performed on >10,000 materials. Using the TQC method, we found 4873 materials with nonatomic phonon band sets. All the materials' data were collected to build the Topological Phonon Database. irreps, irreducible representations.

RESEARCH ARTICLE

TOPOLOGICAL MATTER

Catalog of topological phonon materials

Yuanfeng Xu[1,2]*, M. G. Vergniory[3,4], Da-Shuai Ma[5], Juan L. Mañes[6], Zhi-Da Song[2,7], B. Andrei Bernevig[2,3,8]*, Nicolas Regnault[9,2]*, Luis Elcoro[6]*

Phonons play a crucial role in many properties of solid-state systems, and it is expected that topological phonons may lead to rich and unconventional physics. On the basis of the existing phonon materials databases, we have compiled a catalog of topological phonon bands for more than 10,000 three-dimensional crystalline materials. Using topological quantum chemistry, we calculated the band representations, compatibility relations, and band topologies of each isolated set of phonon bands for the materials in the phonon databases. Additionally, we calculated the real-space invariants for all the topologically trivial bands and classified them as atomic or obstructed atomic bands. We have selected more than 1000 "ideal" nontrivial phonon materials to motivate future experiments. The datasets were used to build the Topological Phonon Database.

A crystalline electronic material is topologically nontrivial if its reciprocal-space Bloch states cannot be expressed in terms of localized Wannier functions (they are not "wannierizable") in real space during an adiabatic process that preserves the crystalline symmetries. In the presence of crystalline or time-reversal symmetries, most of the band topologies can be diagnosed by the Fu-Kane–like topological invariants (*1*) in terms of the band representations at the high-symmetry momenta. Recently, symmetry-protected topological phases in both the 230 paramagnetic and the 1421 magnetic space groups were exhaustively identified by two methods: topological quantum chemistry (TQC) (*2*, *3*) and symmetry-based indicators (*4*–*7*), which facilitated the construction of catalogs of topological bands in both paramagnetic and magnetic electronic materials (*8*–*12*). High-throughput calculations classified >50% of the stoichiometric materials in the Inorganic Crystal Structure Database (*13*) as topological insulators or semimetals at the Fermi level; about 88% had at least one topological band somewhere in the energy spectrum (*12*). In addition to the electronic properties analyzed so far, the phonon structure is another platform for the realization of nontrivial band topologies in solid-state materials. Topological phonons, for instance, play a crucial role in the design of metamaterials with novel properties. The lack of backscattering even in the presence of defects and the existence of one-way edge states under breaking of time-reversal symmetry make the materials with topological phonon states very promising for the construction of phonon diodes (*14*), which conduct phonons in one direction but not in the opposite one, or acoustic waveguides (*15*–*17*). The robustness of the topological surface phonon states can be used for frequency filtering or mechanical energy attenuation under imperfect conditions (*18*), for heat transfer (*19*), and for infrared photoelectronics (*20*). Moreover, there is some evidence of the importance of the electron-phonon coupling in the transport properties of topological semimetals (*21*) and the possible existence of a superconducting phase where the Cooper pairing is mediated by topological phononic edge states (*22*). When time-reversal symmetry is broken, several topological effects, such as quantum anomalous Hall-like or quantum valley Hall-like effects, can be realized in topological phononic materials (*23*).

The gapless nodes of both higher Chern number (*24*–*26*) and non-Abelian charges were predicted in several phonon materials (*27*, *28*). The existence of symmetry-protected topological phases has not been systematically proved in crystalline phonon band structures except for a few isolated cases (*24*–*26*, *29*, *30*) and a brute-force screening of band nodes by calculating the bandgaps along high-symmetry paths in phonon band structures (*31*). The methods of TQC were used to explore the topology of phonons on a particular two-dimensional (2D) lattice (*32*), but no material realizations were predicted. In the present work, we fully extended the application of TQC to phonon systems in all the 3D space groups and systematically completed a catalog of topological phonon bands. On the basis of the dynamical matrices of >10,000 materials that were obtained from ab initio calculations and stored in the Phonon Database at Kyoto University (PhononDB@kyoto-u) (*33*) and the Materials Project database (*34*, *35*), we performed a high-throughput calculation of phonon irreducible representations (irreps), compatibility relations, topological indices, and TQC real-space invariants (RSIs) beyond symmetry indicators (*36*, *37*). We also computed the surface phonon dispersion on different surfaces in all the studied materials. Every isolated set of fully connected bands along all the high-symmetry lines and planes in momentum space was ultimately diagnosed as topologically nontrivial (with strong or fragile topology), as obstructed atomic band representation (OABR, a wannierizable set of bands with at least one Wannier function out of the occupied atomic positions), as orbital-selected OABR (OOABR), or as an atomic (trivial) set of bands (wannierizable bands all located at the occupied atomic positions). As a result of the evaluation of the phonon band structures, we have chosen for future experimental analysis a first set of 935 and 85 phonon materials from the PhononDB@kyoto-u and Materials Project, respectively. These selected materials have at least one nontrivial topology: strong or fragile topological bands, an OABR or OOABR topology, or symmetry-enforced band nodes. In our present work, the meaning of the tag OABR is similar to its meaning in the analysis of an electronic structure. If an isolated set of phononic dispersion bands can be expressed as a linear combination of bands induced from irreps of the site-symmetry groups of a set of Wyckoff positions, but, necessarily, at least one of these Wyckoff positions is empty, then the compound is tagged as OABR. The meaning of the tag OOABR is also similar to its meaning in electronic systems: The set of bands can be induced from irreps of the site-symmetry groups of occupied Wyckoff positions, but at least one irrep does not correspond to the vector representation of one site-symmetry group. Finally, the full list of phonon materials and a wide array of data, including band structures, density of states (DOS), sets of irreps, topology classification, topological indices, and surface states, were collected to build the Topological Phonon Database (*38*).

Workflow of high-throughput calculations

The high-throughput calculations were performed using as input the data deposited in the two phonon material databases, PhononDB@kyoto-u and Materials Project, which store the dynamical matrices for 9991 and 1516 compounds of different Materials Project identification numbers (MPIDs), respectively. A brief overview of the two databases is provided in

[1]Center for Correlated Matter and School of Physics, Zhejiang University, Hangzhou 310058, China. [2]Department of Physics, Princeton University, Princeton, NJ 08544, USA. [3]Donostia International Physics Center, 20018 Donostia–San Sebastian, Spain. [4]Max Planck Institute for Chemical Physics of Solids, 01309 Dresden, Germany. [5]Department of Physics and Chongqing Key Laboratory for Strongly Coupled Physics, Chongqing University, Chongqing 400044, China. [6]Department of Physics, University of the Basque Country UPV/EHU, 48080 Bilbao, Spain. [7]International Center for Quantum Materials, School of Physics, Peking University, Beijing 100871, China. [8]IKERBASQUE, Basque Foundation for Science, 48009 Bilbao, Spain. [9]Laboratoire de Physique de l'École Normale Supérieure, PSL University, CNRS, Sorbonne Université, Université Paris Diderot, Sorbonne Paris Cité, 75005 Paris, France.
*Corresponding author. Email: y.xu@zju.edu.cn (Y.X.); bernevig@princeton.edu (B.A.B.); regnault@princeton.edu (N.R.); luis.elcoro@ehu.eus (L.E.)

section S3 of (*39*). By filtering out the MPIDs that have symmetry inconsistencies, meaning that the dynamical matrix is incompatible with the associated space group, we have designed several modules (as schematically illustrated in Fig. 1) to calculate the phonon irreps and to diagnose the phonon topology of the remaining MPIDs. In this section, we give only an outline of the operation of each module. Further details can be found in section S4 of (*39*).

In step A, the force constants data of each MPID entry were obtained through the inverse Fourier transform of the dynamical matrix, that is, the second-order derivatives of the total energy with respect to atomic displacements on a regular grid of the first Brillouin zone used in the ab initio calculations. The band structures along all high-symmetry paths in the Brillouin zone and DOS were calculated from the force constants data by an interpolation method.

In step B, we calculated the symmetry eigenvalues of phonon vibrational modes at all the high-symmetry momenta [the maximal **q**-vectors (*2*)] and generated the trace.txt file collecting all the symmetry eigenvalues [see section S4, subsection A3, of (*39*) for more details]. Then, we fed all the trace.txt files into the recently implemented utility Check Topological Phonons (*40*) [see section S4, subsection C, of (*39*)], closely related to the program Check Topological Mat. (*41*) for electronic bands (*8*, *12*), which is available online at the Bilbao Crystallographic Server (*42*), and for each file we performed steps C, D, and E (described in the next paragraphs).

In step C, we identified the single-valued irreps (i.e., the irreps without spin-orbit coupling) at the maximal **q**-vectors for all the trace.txt files. The symmetry properties of a set of phonon bands are characterized by the multiplicities of irreps at these maximal **q**-vectors, which form a symmetry data vector.

In step D, we checked the band connectivity along all the high-symmetry paths in the Brillouin zone. A set of states connected along the Brillouin zone build an isolated set of bands if its symmetry data vector satisfies all the compatibility relations, meaning that for every pair q_1 and q_2 of maximal **q**-vectors and the intermediate path q_p that connects both points, the irreps at q_1 and q_2 subduce into the same set of irreps at q_p. Otherwise, the set of eigenstates necessarily has symmetry-enforced band crossings (nodes) with other bands above or below the given set of states and, therefore, does not form an isolated set of bands. In our calculations, we identified all the isolated sets of bands that cannot be further split into subsets that also form isolated bands. Along with the identification of each isolated band by its symmetry data vector, we also stored the symmetry data vector of the cumulative set of bands, that is, the whole set of bands starting from the band with lowest energy up to a given band.

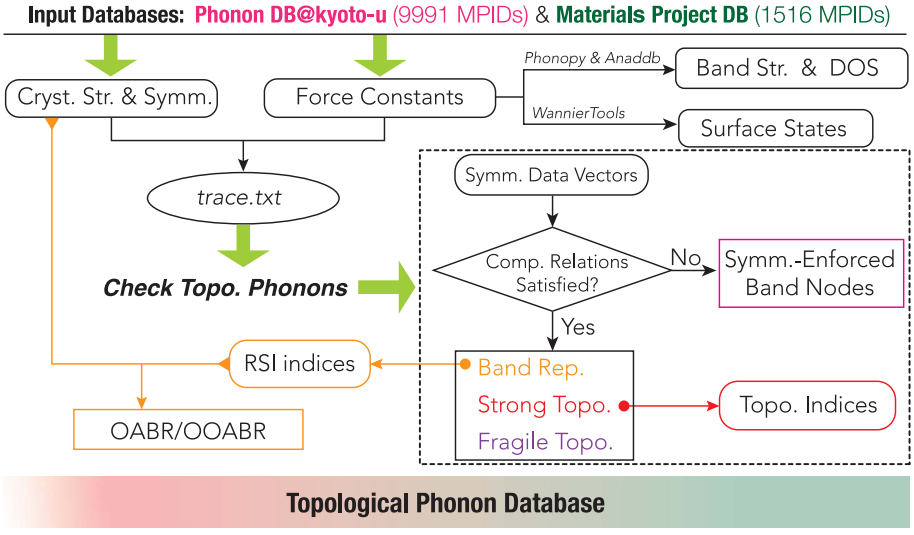

Fig. 1. Workflow scheme of the construction of the Topological Phonon Database. The high-throughput calculations rely on the dynamical matrices of 9991 and 1516 MPID entries in the databases PhononDB@kyoto-u and Materials Project, respectively. We first analyzed the crystal structure and symmetry properties for each entry and filtered out the entries that have symmetry inconsistencies in their dynamical matrix. Through the Fourier transform of the dynamical matrix, we obtained the force constants, which are used to calculate the phonon band structure, the DOS, the symmetry eigenvalues at the high-symmetry momenta (trace.txt file), and the surface states. Lastly, the trace.txt files were fed into the new program called Check Topological Phonons (*40*) to obtain the symmetry data vectors, the isolated sets of bands that satisfy the compatibility relations, the topological properties, and the topological indices. All the materials' data were collected to build the Topological Phonon Database (*38*).

In step E, using the TQC method (*2*, *3*), we identified the topology of each isolated set of bands and also the topology of the cumulative band set. In both cases, we diagnosed bands as having strong topology with topological indices (or symmetry indicators), as having fragile topology, or as a band representation (trivial).

In step F, for all the topologically trivial sets labeled as a band representation, we calculated their RSIs, which indicate the location of the corresponding Wannier functions in real space. A set of bands is referred to as OABR when its RSI is nonzero at a Wyckoff position that is not occupied by atoms (*2*, *36*, *37*, *43*, *44*). If the nonzero RSIs are located at occupied Wyckoff positions, but the orbitals that define the RSI do not correspond to the vector representation of the site-symmetry group (the representation of the p orbitals), the related set of bands are labeled as an OOABR (*37*).

The main advantage of the method described above with respect to the brute-force analysis of (*31*) is the computation time required and the minimization of cutoff problems. Starting from the same input raw data (step A), the method developed in (*31*) needs the analysis of differences in energy along all the high-symmetry lines in a relatively dense k-grid to identify possible band crossings, that is, energy differences below the chosen cutoff. When a gapped set of bands has been identified, one must compute the Berry phase by the integral of the Berry connection to discriminate topological bands from trivial ones. Using the method described in steps B to F above, we computed the traces of the symmetry operators in a very small number of points (maximal **k**-vectors that range from 4 to 8, depending on the space group) and identified the irreps associated with each degenerate set of eigenstates. Then, using the tabulated compatibility relations between each pair of high-symmetry **k**-vectors, we could determine whether there must be a band crossing in the intermediate path and, when there was no such crossing, we could immediately identify the topological character of the set of bands.

For semiconductor materials of polar crystal structures, the long-range macroscopic electric field induced by long-wavelength longitudinal optical (LO) phonons is usually non-negligible (*45*). The coupling between LO mode and electric fields is a nonanalytical correction (NAC) to the dynamical matrix (*46*, *47*), resulting in an energy difference between the LO mode and the transverse optical (TO) mode [see section S4, subsection A2, in (*39*) for a formal definition of NAC]. In general, this LO-TO splitting destroys the continuity of the phonon spectrum when approaching the center of the Brillouin zone ($q = 0$) along different directions. For a special case, the energy order of two bands (of different band representations) could be inverted by the LO-TO splitting at a finite momentum

close to the Γ point (the center of the Brillouin zone) with respect to the band order at Γ (this inversion can happen owing to the mentioned discontinuity). In the TQC high-throughput method, only the information obtained at the maximal **q**-vectors is used to identify the topology of a given set of bands. As a consequence, the potential band inversion caused by the LO-TO splitting can be missed, and the topological classification might be wrong. One specific example of sets of phonon bands that change type thanks to NAC is the material Dy_2O_3 [MPID = mp-555574, SG 12 ($C2/m$)]. Without NAC, the first two subsets of bands of lowest energy have 11 and 2 bands, respectively. Both subsets are identified as topological, but the cumulative full set of 13 bands is trivial. However, with NAC, at the A and M maximal **k**-vectors, two eigenstates (one from each subset) swap ($A_1^+ \leftrightarrow A_2^-$ and $M_2^+ \leftrightarrow M_2^-$, respectively). In this new configuration, the first 11 sets of irreps do not fulfill the compatibility relations in every pair of maximal **k**-vectors, and then the 11+2 sets of bands without NAC transform with NAC into a single set of connected 13 bands, tagged as trivial. A full analysis on the differences with and without NAC calculations and detailed statistics are provided in section S7 of (*39*). We have also applied the TQC method to phonons with NAC and provide the results for reference.

Although the topological surface states in electronic materials have been detected by several spectroscopic and transport experiments, the related experiments on topological phonon surface states are rare. First, the experimental technique of surface phonon detection is limited to electron energy loss spectroscopy, whose energy resolution is between 5 and 10 meV, making the surface phonon modes difficult to resolve. Second, a topological phonon material database with surface phonon spectrum to serve as a guideline to experiments was so far unavailable. In the present work, we have also developed a high-throughput algorithm for the calculation of phonon surface states. The method is detailed in section S5 of (*39*), and the algorithm has been embedded with the WannierTools software package (*48*). For each phonon material, we select three nonequivalent cleavage planes and calculate their surface states with a finite-size slab structure. For further detailed calculations and analysis of the phonon surface states, we have provided the WannierTools input files for each MPID entry in the Topological Phonon Database (*38*).

Topological data analysis

Material database and statistics

By applying the above high-throughput screening method, we have successfully identified the band representations and band topologies for 9991 MPID entries in PhononDB@kyoto-u and 1516 MPID entries in the Materials Project. As the ab initio calculations were performed on a finite-size supercell structure (for PhononDB@kyoto-u) or a less dense mesh grid in the Brillouin zone, the resulting phonon band structures usually host imaginary frequencies in a partial region of the Brillouin zone, related to negative eigenvalues of the dynamical matrix. In section S7, subsection B, of (*39*), we tag the materials with a minimum frequency lower than −5 meV as MPID entries with "negativity" issues. Depending on the features of these imaginary frequencies in the phonon spectrum with NAC, we manually divide the MPIDs with "negativities" into three categories: "interpolation error," when a weak negativity over part of the Brillouin zone results from interpolation errors; "instability," indicating that a potential structural phase transition might occur at a lower temperature; and "discarded," when a strong negativity is present over most of or the entire Brillouin zone. The interpolation error can potentially be fixed by requiring a higher accuracy [see the detailed analysis of this type of error in section S7, subsection B, of (*39*)].

By filtering out the MPIDs that have a "negativity" tag in the calculations with NAC, we were left with 7983 (versus 7809 in the calculations without NAC) and 1394 (versus 1389 in the calculations without NAC) "high-quality" phonon band structures in PhononDB@kyoto-u and Materials Project, respectively. Figure 2 summarizes the statistics of materials hosting nonatomic band sets, that is, either strong topology, fragile topology, OABR, or OOABR. Notably, about half of the materials host at least one nonatomic cumulative band set: 47.66% of the materials from the Materials Project and 53.92% of those from PhononDB@kyoto-u. In section S7, subsection C, of (*39*), we provide an in-depth discussion of statistics, with or without NAC, and with or without the materials with imaginary frequencies.

The percentage of materials hosting nonatomic phonon band sets, although substantial, is not as high as the percentage of materials hosting topological electronic bands with spin-orbit coupling [87.99% as reported in (*12*)] but is actually higher than the percentage of materials hosting topological electronic bands without spin-orbit coupling [27.66% as reported in (*12*)]. Also, the main contribution to the percentage of topological band sets strongly differs in electronic and phononic band structures. As illustrated in Fig. 2, there is an abundance of materials with trivial but nonatomic cumulative phonon band sets, that is, either OABR or OOABR. A qualitative explanation can be found by considering swap optical vibrational modes. Indeed, if we consider the simplest case of a 1D system with inversion symmetry, the optical (or acoustic) mode contributed by the atoms at 2c (i.e., the general Wyckoff position) has to be obstructed (OABR or OOABR) at one of the inversion centers (1a or 1b) whether or not the center is occupied by an atom. It should thus be expected that OABR and OOABR are common in phonon band structures. As a side note, we observe a near absence of fragile cumulative topology for phonons.

Interpretation of the topological indices

For each (isolated and cumulative) topological set of bands, we have calculated its topological indices (*2*–*6*, *49*). As proved in (*49*), although the band structures along all the high-symmetry paths satisfy all the compatibility relations, the nonzero topological indices defined in

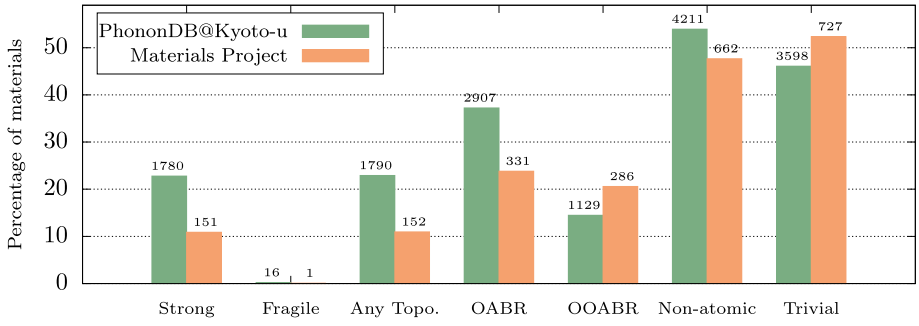

Fig. 2. Statistics of nontrivial phonon band sets for the phonon materials from PhononDB@kyoto-u (green) and Materials Project (orange). All numbers and percentages are from the calculations without NAC and without the materials tagged as having imaginary phonon frequencies. The number above each bar is the number of materials for each category and data source. From left to right: "Strong" and "Fragile" refer to materials hosting at least one cumulative band set of strong and fragile topology, respectively. "Any Topo." corresponds to materials hosting at least one cumulative band set that has either strong or fragile topology. "OABR" and "OOABR" give similar figures for OABR and OOABR band sets, whereas "Nonatomic" stands for the number of materials hosting at least one nonatomic cumulative band set, that is, strong topology, fragile topology, OABR, or OOABR. Note that a material can host several types of nontrivial or nonatomic band sets. Thus, the percentages do not add up. Finally, "Trivial" gives the number of materials having solely atomic cumulative band sets.

spinless space groups (namely without spin-orbit coupling) are necessarily indicating gapless band nodes (points or lines). Compared with the symmetry-enforced band nodes, which break the compatibility relations, symmetry-indicated band nodes occur in general at generic momenta in the Brillouin zone. It was also proved in (*49*) that all the nontrivial topological indices in (non)centrosymmetric space groups indicate nodal lines (Weyl nodes). A more detailed analysis of the physical consequences of the topological indices and different band topologies can be found in section S2, subsection C, of (*39*). Notably, in 33 of the 41 centrosymmetric space groups that have topological indices well defined in TQC, there is always at least one set of indices that indicates the presence of nodal lines with Z_2-monopole charge. For each set of topological bands in the Topological Phonon Database, we have tabulated the essential topological indices that were defined and physically interpreted in (*49*). Once the MPIDs tagged as having imaginary phonon frequencies have been removed from the final list, we find 1780 (22.79%) entries in PhononDB@kyoto-u and 151 (10.87%) entries in Materials Project that have all kinds of symmetry-indicated spinless topologies, including Weyl nodes, and nodal lines with and without Z_2-monopole charge.

Notable topological phonon materials

"Ideal" phonon materials with nonatomic cumulative topologies

The Topological Phonon Database allows the search for the most-promising candidates, exhibiting any of the nonatomic properties and additional criteria, detailed in section S8 of (*39*), where the main results of the search are also presented. In addition to hosting either a nonatomic bandgap or symmetry-enforced band nodes, we imposed the following restrictions for a material to be considered "ideal": (i) The material is not tagged as having "negativities" in the database, meaning that its minimum energy is above −5.0 meV, so that the

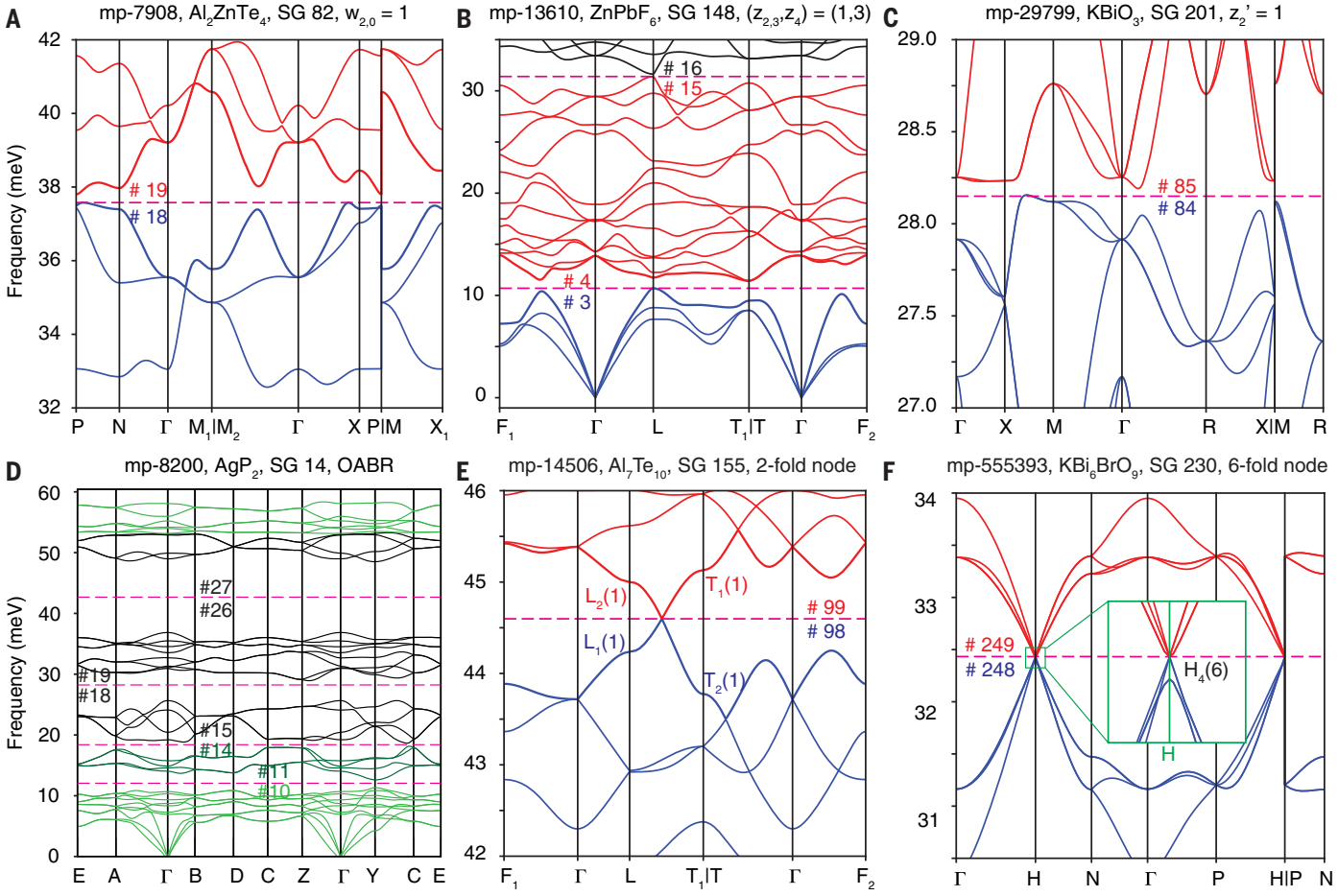

Fig. 3. Phonon band dispersion of our relation of six prototypical materials. (**A**) Al_2ZnTe_4. An ideal topological bandgap is between bands 18 and 19, where blue and red bands are below and above the topological gap, respectively. Topological index of the blue bands is $\omega_{2,0} = 1$, indicating four Weyl points on the $k_z = 0$ slice. (**B**) $ZnPbF_6$. There are two ideal topological bandgaps: One is located between bands 3 and 4 and the other between bands 15 and 16. Symmetry data vectors of bands below the two gaps have the same set of topological indices $(z_{2,3}, z_4) = (1,3)$, indicating nodal lines of π-Berry phase. (**C**) $KBiO_3$. The topological band gap between bands 84 and 85 has a topological index $z_{2'} = 1$, indicating three pairs of Z_2-monopole charge nodal lines. (**D**) AgP_2. There are three isolated band sets [plotted in light green (1 to 10), dark green (11 to 14), and light green (31 to 36) lines, respectively] diagnosed as OABR topology. The calculation of the (cumulative) RSIs up to a given band shows that there are four cumulative band sets hosting both an OABR topology and an indirect bandgap (indicated by the pink dashed lines). (**E**) Al_7Te_{10}. The first 98 sets of irreps at maximal **q**-vectors do not form a fully connected set of bands. The irreps of band 98 (99) at the L and T points are $L_1(1)$ and $T_2(1)$ [$L_2(1)$ and $T_1(1)$], respectively. Owing to the compatibility relations along the intermediate L–Y–T path, $L_1(1)$ is connected to $T_1(1)$, and $L_2(1)$ is connected to $T_2(1)$. There is thus a symmetry-enforced band crossing between bands 98 and 99, giving a twofold Weyl node. Note that the number in parentheses is the dimension of the corresponding irrep. (**F**) KBi_6BrO_9. There is a sixfold degeneracy point at Γ, composed of bands 247 to 252. The six-dimensional irrep (H_4) is protected by inversion symmetry, threefold rotation symmetry along the (111) direction, fourfold rotation symmetry combined with a fractional translation $\{C_{4z}|(\frac{1}{4},\frac{3}{4},\frac{1}{4})\}$, and a twofold screw symmetry $\{C_{2y}|(\frac{1}{2},0,0)\}$ (*57*).

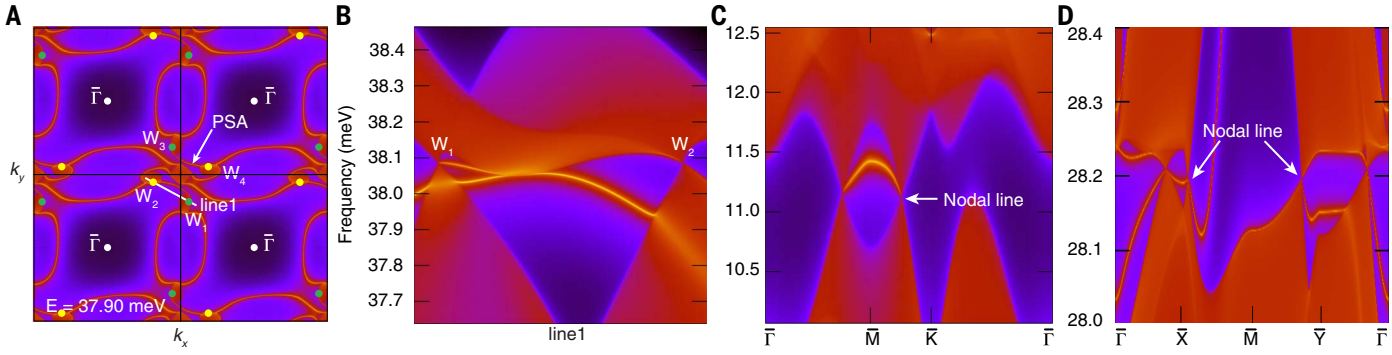

Fig. 4. Surface-state calculations for three prototypical topological phonon materials. (**A** and **B**) Surface-state calculation for Al_2ZnTe_4 on the (001) surface. (A) Energy contour (E = 37.9 meV) of the surface states in a 2-by-2 surface Brillouin zone, where the locations of Weyl points with chirality +1 (−1) are indicated by the green (yellow) dots. Surface-state dispersion along the path that connects the two Weyl points W_1 and W_2 is shown in (B). The topological phonon surface arc (PSA) states can be distinguished from the bulk states in both (A) and (B). (**C**) Drumhead-like surface states of $ZnPbF_6$ on the (001) surface. The nodal line bulk states are formed by the band crossing between bands 3 and 4, which is indicated by the nontrivial topological indices ($z_{2,3}$, z_4) = (1,3) in SG 148. (**D**) Drumhead-like surface states connecting the topological nodal lines of Z_2-monopole charge on the (001) surface of $KBiO_3$. The nodal lines are formed by the band crossing between bands 84 and 85, indicated by the nontrivial topological index w_2 = 1 in SG 201.

crystal structure is considered relatively stable. (ii) The maximal direct bandgap along all the high-symmetry paths between the nonatomic cumulative set of bands and the first band above it (or between the bands forming a symmetry-enforced band node) is larger than 1 meV, which is the typical experimental resolution to distinguish a phonon bandgap. (iii) The indirect gap along all the high-symmetry paths is positive for nonatomic cumulative band sets and nonnegative for symmetry-enforced band nodes, respectively.

Applying these three additional filtering criteria, we obtained 187 (1.63%), 1430 (12.43%), and 623 (5.41%) "ideal" phonon materials with strong, OABR, and OOABR topologies, respectively. Additionally, we selected 846 (7.35%) phonon materials hosting "ideal" symmetry-enforced band nodes. Note that we find no "ideal" phonon material with fragile cumulative topology satisfying the above criteria, which is unsurprising owing to the near absence of fragile cumulative topology as discussed previously. The material lists and statistics for each type of "ideal" materials in both PhononDB@kyoto-u and Materials Project are detailed in section S8, subsection A, of (*39*). Moreover, in section S8, subsection B, of (*39*), we provide the phonon spectrum plot near the topological bandgap and band nodes for "ideal" materials with strong topologies and symmetry-enforced band nodes.

Prototypical topological phonon materials

To stimulate the relevant experimental investigation, we here highlight six representative "ideal" phonon materials with symmetry-indicated topological bands, OABR bands, or symmetry-enforced band nodes. The six materials are Al_2ZnTe_4 [MPID = mp-7908, SG 82 ($I\bar{4}$)], $ZnPbF_6$ [MPID = mp-13610, SG 148 ($I4_1/acd$)], $KBiO_3$ [MPID = mp-29799, SG 201 ($Pn\bar{3}$)], AgP_2 [MPID = mp-8200, SG 14 ($P2_1/c$)], Al_7Te_{10} [MPID = mp-14506, SG 155 ($R32$)], and KBi_6BrO_9 [MPID = mp-555393, SG 230 ($Ia\bar{3}d$)]. As shown in Fig. 3, the first three materials have symmetry-indicated topological bands, AgP_2 has three OABR-topology isolated band sets, and the last two materials have symmetry-enforced band nodes. Details about the topological properties and surface-state calculations of these materials are provided in section S6 of (*39*). In the following paragraphs, we briefly discuss the nonatomic bands in Al_2ZnTe_4, $KBiO_3$, and AgP_2.

In the phonon band structure of noncentrosymmetric Al_2ZnTe_4 (Fig. 3A), the cumulative band set of indices 1 to 18 is topological, as indicated by a Z_2 index $\omega_{2,0}$ = 1. In (*49*), $\omega_{2,0} \times \pi$ is interpreted as the Berry phase of a loop enclosing a quarter of the Brillouin zone at the k_z = 0 plane (which is invariant under a four-fold rotation). Hence, $\omega_{2,0}$ = 1 indicates 4 mod 8 Weyl points in between bands 18 and 19 on the k_z = 0 slice. More details about the topological index, Weyl points, and surface state (phonon surface arc) calculations are provided in section S6, subsection A, of (*39*).

$KBiO_3$ crystallizes in the centrosymmetric space group $Pn\bar{3}$. As shown in Fig. 3C, the cumulative band set of indices 1 to 84 has a nonzero topological index $z_{2'}$ = 1, which indicates three pairs of nodal lines of Z_2-monopole charge caused by the C_3 symmetry, according to (*49*). Unlike the π-Berry phase nodal line (which is also indicated by nonzero topological indices), Z_2-monopole charge nodal line has to be created (or annihilated) in pairs and is characterized by the second Stiefel-Whitney class, which is indicated by a Z_2 indicator w_2 and can be read off from the Wilson loop spectrum (*50*, *51*). In section S6, subsection C, of (*39*), we calculate the Wilson-loop evolution for this cumulative band set on a 2D closed manifold wrapping a nodal line, where an odd number of crossing points at Wannier charge center (WCC) = π line corresponds to a w_2 = 1 phase and indicates the Z_2-monopole charge.

In the phonon spectrum of AgP_2 (from the Kyoto database) shown in Fig. 3D, there are six cumulative band sets and three isolated band sets (the green bands) that have an OABR topology, among which four cumulative band sets have an indirect bandgap (indicated by the pink dashed lines). The nonzero RSIs of these three isolated band sets are $\delta_1(a)$ = 1 for band set 1 to 10, $\{\delta_1(a) = -1, \delta_4(d) = 1\}$ for band set 11 to 14, and $\delta_4(d) = -1$ for band set 31 to 36, where a nonzero RSI $\delta(w)$ implies unavoidable Wannier functions at the Wyckoff position w (i.e., a or d), and neither a nor d are occupied by any atom. The RSIs of each cumulative band set can be obtained simply by summing the RSIs of all the isolated band sets within it.

In Fig. 4, we show the results of the surface-state calculations using the Green's function method (*52*) for the three symmetry-indicated topological phonon bands in the first row of Fig. 4, namely, Al_2ZnTe_4 with two pairs of Weyl nodes as shown in Fig. 4, A and B, $ZnPbF_6$ with topological nodal line of π-Berry phase (Fig. 4C), and $KBiO_3$ (Fig. 4D) with topological nodal line of Z_2-monopole charge. In the energy contour and dispersion plots, the phonon surface arc connecting one pair of Weyl nodes and the drumhead-like surface states connecting the nodal lines can be distinguished. In section S6 of (*39*), we provide additional surface-state calculations with different surface terminations for these three materials.

Discussion and outlook

We have performed a comprehensive topological classification for >10,000 phonon materials in a high-throughput search, and we have made the results available at our public website, the Topological Phonon Database (*38*).

We identified the band representations and topology of each phonon band set by calculating the topological indices and RSIs. Similar to the findings for the electronic structures of solid-state materials, nontrivial band topologies are ubiquitous in phonon systems: 52.98% of the curated materials have some kind of nontrivial topology. Notably, we predict >1000 phonon materials that have at least one "ideal" nonatomic phonon band set. These ideal materials constitute a valuable platform for further in-depth theoretical and experimental studies about phonon-band topologies. Although we did not find any phonon materials hosting "ideal" band sets with both cumulative fragile topology and finite indirect bandgap, there exist several materials with perfect isolated fragile band sets, such as the $C_2 \cdot T$-symmetry–protected fragile band sets in HfIN [MPID = mp-567441, SG 166 ($R\bar{3}m$)] discussed in section S6, subsection E, of (*39*). As phonons are bosonic excitations, topological bandgaps (or nodes) are not limited to a specific energy level, and the nontrivial topology at any frequency level could be of interest and detectable in experiments. On the basis of the formalism and results of this work, future extension of the catalog of topological phonons will encompass all the solid-state materials contained in the Inorganic Crystal Structure Database (*13*). The results of the present work, together with the previous complete analysis of the band topology of the electronic states (*8*–*10*, *12*), will be useful in the analysis of the consequences of the electron-phonon coupling on the physical properties of the materials when the topology of both subsystems come into play.

Methods

The phonon band structures were calculated with Phonopy version 2.14 (*53*) and ANADDB version 8.10.1 (*54*–*56*) software packages, and the phonon surface states were calculated with WannierTools package (*48*). The phonon trace.txt files were calculated with the phonopy2trace package as embedded in the program Check Topological Phonons (*40*).

The high-throughput calculations of phonon surface states are performed by constructing a slab-structure finite-size unit cell, whose thickness is >100 Å along the open-boundary direction, which is large enough to avoid the coupling between the top and bottom surfaces. The Miller indices of the open-boundary surfaces and high-symmetry k-paths used in the slab calculations are detailed in section S5 of (*39*).

REFERENCES AND NOTES

1. L. Fu, C. L. Kane, E. J. Mele, Topological insulators in three dimensions. *Phys. Rev. Lett.* **98**, 106803 (2007). doi: 10.1103/PhysRevLett.98.106803; pmid: 17358555
2. B. Bradlyn *et al*., Topological quantum chemistry. *Nature* **547**, 298–305 (2017). doi: 10.1038/nature23268; pmid: 28726818
3. L. Elcoro *et al*., Magnetic topological quantum chemistry. *Nat. Commun.* **12**, 5965 (2021). doi: 10.1038/s41467-021-26241-8; pmid: 34645841
4. H. C. Po, A. Vishwanath, H. Watanabe, Symmetry-based indicators of band topology in the 230 space groups. *Nat. Commun.* **8**, 50 (2017). doi: 10.1038/s41467-017-00133-2; pmid: 28667305
5. H. Watanabe, H. C. Po, A. Vishwanath, Structure and topology of band structures in the 1651 magnetic space groups. *Sci. Adv.* **4**, eaat8685 (2018). doi: 10.1126/sciadv.aat8685; pmid: 30083612
6. J. Kruthoff, J. de Boer, J. van Wezel, C. L. Kane, R.-J. Slager, Topological classification of crystalline insulators through band structure combinatorics. *Phys. Rev. X* **7**, 041069 (2017). doi: 10.1103/PhysRevX.7.041069
7. Z. Song, Z. Fang, C. Fang, (d − 2)-Dimensional edge states of rotation symmetry protected topological states. *Phys. Rev. Lett.* **119**, 246402 (2017). doi: 10.1103/PhysRevLett.119.246402; pmid: 29286745
8. M. G. Vergniory *et al*., A complete catalogue of high-quality topological materials. *Nature* **566**, 480–485 (2019). doi: 10.1038/s41586-019-0954-4; pmid: 30814710
9. T. Zhang *et al*., Catalogue of topological electronic materials. *Nature* **566**, 475–479 (2019). doi: 10.1038/s41586-019-0944-6; pmid: 30814713
10. F. Tang, H. C. Po, A. Vishwanath, X. Wan, Comprehensive search for topological materials using symmetry indicators. *Nature* **566**, 486–489 (2019). doi: 10.1038/s41586-019-0937-5; pmid: 30814709
11. Y. Xu *et al*., High-throughput calculations of magnetic topological materials. *Nature* **586**, 702–707 (2020). doi: 10.1038/s41586-020-2837-0; pmid: 33116291
12. M. G. Vergniory *et al*., All topological bands of all nonmagnetic stoichiometric materials. *Science* **376**, eabg9094 (2022). doi: 10.1126/science.abg9094; pmid: 35587971
13. G. Bergerhoff, R. Hundt, R. Sievers, I. D. Brown, The inorganic crystal structure data base. *J. Chem. Inf. Comput. Sci.* **23**, 66–69 (1983). doi: 10.1021/ci00038a003
14. Y. Liu, Y. Xu, S.-C. Zhang, W. Duan, Model for topological phononics and phonon diode. *Phys. Rev. B* **96**, 064106 (2017). doi: 10.1103/PhysRevB.96.064106
15. P. Wang, L. Lu, K. Bertoldi, Topological phononic crystals with one-way elastic edge waves. *Phys. Rev. Lett.* **115**, 104302 (2015). doi: 10.1103/PhysRevLett.115.104302; pmid: 26382680
16. Y. Guo, T. Dekorsy, M. Hettich, Topological guiding of elastic waves in phononic metamaterials based on 2D pentamode structures. *Sci. Rep.* **7**, 18043 (2017). doi: 10.1038/s41598-017-18394-8; pmid: 29273741
17. V. Laude, Principles and properties of phononic crystal waveguides. *APL Mater.* **9**, 080701 (2021). doi: 10.1063/5.0059035
18. Z. Xiong *et al*., Topological node lines in mechanical metacrystals. *Phys. Rev. B* **97**, 180101 (2018). doi: 10.1103/PhysRevB.97.180101
19. B. Wang, C. Zhao, Topological phonon polariton enhanced radiative heat transfer in bichromatic nanoparticle arrays mimicking Aubry-André-Harper model. *Phys. Rev. B* **107**, 125409 (2022). doi: 10.1103/PhysRevB.107.125409
20. C. R. Gubbin, S. De Liberato, T. G. Folland, Surface phonon polaritons for infrared optoelectronics. *J. Appl. Phys.* **131**, 030901 (2022). doi: 10.1063/5.0064234
21. G. B. Osterhoudt *et al*., Evidence for dominant phonon-electron scattering in Weyl semimetal WP_2. *Phys. Rev. X* **11**, 011017 (2021). doi: 10.1103/PhysRevX.11.011017
22. D. Di Miceli, C. Setty, A. Zaccone, Theory of superconductivity mediated by topological phonons. *Phys. Rev. B* **106**, 054502 (2022). doi: 10.1103/PhysRevB.106.054502
23. Y. Liu, X. Chen, Y. Xu, Topological phononics: From fundamental models to real materials. *Adv. Funct. Mater.* **30**, 1904784 (2020). doi: 10.1002/adfm.201904784
24. T. Zhang *et al*., Double-Weyl phonons in transition-metal monosilicides. *Phys. Rev. Lett.* **120**, 016401 (2018). doi: 10.1103/PhysRevLett.120.016401; pmid: 29350958
25. H. Miao *et al*., Observation of double Weyl phonons in parity-breaking FeSi. *Phys. Rev. Lett.* **121**, 035302 (2018). doi: 10.1103/PhysRevLett.121.035302; pmid: 30085785
26. T. T. Zhang *et al*., Phononic helical nodal lines with PT protection in MoB_2. *Phys. Rev. Lett.* **123**, 245302 (2019). doi: 10.1103/PhysRevLett.123.245302; pmid: 31922848
27. B. Peng, A. Bouhon, B. Monserrat, R.-J. Slager, Phonons as a platform for non-Abelian braiding and its manifestation in layered silicates. *Nat. Commun.* **13**, 423 (2022). doi: 10.1038/s41467-022-28046-9; pmid: 35058473
28. B. Peng, A. Bouhon, R.-J. Slager, B. Monserrat, Multigap topology and non-Abelian braiding of phonons from first principles. *Phys. Rev. B* **105**, 085115 (2022). doi: 10.1103/PhysRevB.105.085115
29. G. Liu, Y. Jin, Z. Chen, H. Xu, Symmetry-enforced straight nodal-line phonons. *Phys. Rev. B* **104**, 024304 (2021). doi: 10.1103/PhysRevB.104.024304
30. J. Zhu *et al*., Symmetry-enforced nodal chain phonons. *NPJ Quantum Mater.* **7**, 52 (2022). doi: 10.1038/s41535-022-00461-7
31. J. Li *et al*., Computation and data driven discovery of topological phononic materials. *Nat. Commun.* **12**, 1204 (2021). doi: 10.1038/s41467-021-21293-2; pmid: 33619273
32. J. L. Mañes, Fragile phonon topology on the honeycomb lattice with time-reversal symmetry. *Phys. Rev. B* **102**, 024307 (2020). doi: 10.1103/PhysRevB.102.024307
33. PhononDB@kyoto-u; https://github.com/atztogo/phonondb.
34. Materials Project; https://next-gen.materialsproject.org.
35. G. Petretto *et al*., High-throughput density-functional perturbation theory phonons for inorganic materials. *Sci. Data* **5**, 180065 (2018). doi: 10.1038/sdata.2018.65; pmid: 29714723
36. Z.-D. Song, L. Elcoro, B. A. Bernevig, Twisted bulk-boundary correspondence of fragile topology. *Science* **367**, 794–797 (2020). doi: 10.1126/science.aaz7650
37. Y. Xu *et al*., Three-dimensional real space invariants, obstructed atomic insulators and a new principle for active catalytic sites. arXiv:2111.02433 [cond-mat.mtrl-sci] (2021).
38. Topological Phonon Database; https://www.topologicalquantumchemistry.fr/topophonons.
39. See supplementary materials.
40. Check Topological Phonons; https://www.cryst.ehu.es/cgi-bin/cryst/programs/magnetictopo.pl?tipog=phonon.
41. Check Topological Mat.; https://www.cryst.ehu.es/cgi-bin/cryst/programs/magnetictopo.pl?tipog=gesp.
42. Bilbao Crystallographic Server; https://www.cryst.ehu.es.
43. Y. Xu *et al*., Filling-enforced obstructed atomic insulators. *Phys. Rev. B* **109**, 165139 (2024).
44. J. Gao *et al*., Unconventional materials: The mismatch between electronic charge centers and atomic positions. *Sci. Bull. (Beijing)* **67**, 598–608 (2022). doi: 10.1016/j.scib.2021.12.025; pmid: 36546121
45. S. Baroni, S. de Gironcoli, A. Dal Corso, P. Giannozzi, Phonons and related crystal properties from density-functional perturbation theory. *Rev. Mod. Phys.* **73**, 515–562 (2001). doi: 10.1103/RevModPhys.73.515
46. X. Gonze, C. Lee, Dynamical matrices, Born effective charges, dielectric permittivity tensors, and interatomic force constants from density-functional perturbation theory. *Phys. Rev. B* **55**, 10355–10368 (1997). doi: 10.1103/PhysRevB.55.10355
47. Y. Wang *et al*., A mixed-space approach to first-principles calculations of phonon frequencies for polar materials. *J. Phys. Condens. Matter* **22**, 202201 (2010). doi: 10.1088/0953-8984/22/20/202201; pmid: 21393699
48. Q. Wu, S. Zhang, H.-F. Song, M. Troyer, A. A. Soluyanov, WannierTools: An open-source software package for novel topological materials. *Comput. Phys. Commun.* **224**, 405–416 (2018). doi: 10.1016/j.cpc.2017.09.033
49. Z. Song, T. Zhang, C. Fang, Diagnosis for nonmagnetic topological semimetals in the absence of spin-orbital coupling. *Phys. Rev. X* **8**, 031069 (2018). doi: 10.1103/PhysRevX.8.031069
50. C. Fang, Y. Chen, H.-Y. Kee, L. Fu, Topological nodal line semimetals with and without spin-orbital coupling. *Phys. Rev. B* **92**, 081201 (2015). doi: 10.1103/PhysRevB.92.081201
51. J. Ahn, D. Kim, Y. Kim, B.-J. Yang, Band topology and linking structure of nodal line semimetals with Z_2 monopole charges. *Phys. Rev. Lett.* **121**, 106403 (2018). doi: 10.1103/PhysRevLett.121.106403; pmid: 30240267
52. M. L. Sancho, J. L. Sancho, J. L. Sancho, J. Rubio, Highly convergent schemes for the calculation of bulk and surface Green functions. *J. Phys. F Met. Phys.* **15**, 851–858 (1985). doi: 10.1088/0305-4608/15/4/009
53. A. Togo, I. Tanaka, First principles phonon calculations in materials science. *Scr. Mater.* **108**, 1–5 (2015). doi: 10.1016/j.scriptamat.2015.07.021
54. X. Gonze *et al*., First-principles computation of material properties: The ABINIT software project. *Comput. Mater. Sci.* **25**, 478–492 (2002). doi: 10.1016/S0927-0256(02)00325-7
55. X. Gonze *et al*., ABINIT: First-principles approach to material and nanosystem properties. *Comput. Phys. Commun.* **180**, 2582–2615 (2009). doi: 10.1016/j.cpc.2009.07.007

56. X. Gonze *et al*., Recent developments in the ABINIT software package. *Comput. Phys. Commun.* **205**, 106–131 (2016). doi: 10.1016/j.cpc.2016.04.003
57. B. Bradlyn *et al*., Beyond Dirac and Weyl fermions: Unconventional quasiparticles in conventional crystals. *Science* **353**, aaf5037 (2016). doi: 10.1126/science.aaf5037; pmid: 27445310
58. Y. Xu *et al*., Data for "Catalog of topological phonon materials," version 1, Zenodo (2023); https://doi.org/10.5281/zenodo.7670140.

ACKNOWLEDGMENTS

We thank A. Togo, S. Dwaraknath, and K. A. Persson for the helpful discussion about the phonon material databases. Y.X. thanks S. Zhang, X. Jia, and C. Liu for the helpful discussion about experimental detection of phonon topologies. We acknowledge the computational resources Cobra/Draco in the Max Planck Computing and Data Facility (MPCDF). **Funding:** Y.X. was supported by the National Natural Science Foundation of China (General Program no. 12374163) and by the Office of Naval Research (ONR grant no. N00014-20-1-2303). N.R. was supported by US Department of Energy grant no. DE-SC0016239, the Princeton Global Network Funds, and the European Research Council (ERC) under the European Union's Horizon 2020 research and innovation program (grant agreement no. 101020833). B.A.B. was supported by a Simons Investigator grant (no. 404513), the Office of Naval Research (ONR grant no. N00014-20-1-2303), the Schmidt Fund for Innovative Research, the BSF Israel US foundation (grant no. 2018226), the Gordon and Betty Moore Foundation through grant no. GBMF8685 toward the Princeton theory program and grant no. GBMF11070 toward the EpiQS Initiative, and NSF-MRSEC (grant no. DMR-2011750). L.E. was supported by the Government of the Basque Country (Project IT1458-22), the Spanish Ministry of Science and Innovation (PID2019-106644GB-I00), and the ERC under the European Union's Horizon 2020 research and innovation program (grant agreement no. 101020833). M.G.V. acknowledges the Spanish Ministerio de Ciencia e Innovación (grant PID2022-142008NB-I00), the Deutsche Forschungsgemeinschaft (DFG, German Research Foundation) GA 3314/1-1–FOR 5249 (QUAST), and the ERC under the European Union's Horizon 2020 research and innovation program (grant agreement no. 101020833). The work of J.L.M. was supported in part by the Basque Government Grant no. IT1628-22 and the PID2021-123703NB-C21 grant funded by MCIN/AEI/10.13039/501100011033 and by ERDF "A way of making Europe." Z.-D.S. acknowledges the National Natural Science Foundation of China (General Program no. 12274005) and the National Key Research and Development Program of China (no. 2021YFA1401900). D.-S.M. acknowledges the National Natural Science Foundation of China (grant no. 12204074) and the China National Postdoctoral Program for Innovative Talent (grant no. BX20220367). **Author contributions:** B.A.B. and Y.X. conceived of the study. Y.X. developed the code and performed the high-throughput calculations. D.-S.M. prepared the input files for surface-state calculations and performed the ab initio calculations for SnO in the supplementary materials. L.E. and Y.X. performed the topological classifications. N.R. built the Topological Phonon Database with input data from Y.X. and L.E. Y.X., N.R., L.E., M.G.V., Z.-D.S., J.L.M., and B.A.B. analyzed the results and wrote the original draft. Y.X. and N.R. wrote the supplementary materials. All authors contributed to review and editing of the final draft. **Competing interests:** The authors declare that they have no competing interests. **Data and materials availability:** The phonon rawdata of PhononDB@kyoto-u and Materials Project are stored at (*33*) and (*34*), respectively. The phonopy2trace and Check Topological Phonons program can be accessed from (*40*). WannierTools package is available at https://github.com/quanshengwu/wannier_tools. All data are available in the supplementary materials, through our public website Topological Phonon Database (*38*), and in Zenodo (*58*).

SUPPLEMENTARY MATERIALS

science.org/doi/10.1126/science.adf8458
Supplementary Text
Figs. S1 to S184
Tables S1 to S21
References (*59*–*79*)

Submitted 17 November 2022; accepted 20 March 2024
10.1126/science.adf8458